Numerical Simulation of the Scavenging Rates of Ice Crystals of Various Microphysical Characteristics

Richard L. Pitter and *Renyi Zhang*
Atmospheric Sciences Center, Desert Research Institute
University of Nevada System, Reno, Nevada 89506 U. S. A.
Received September 12, 1989; revised September 17, 1990

ABSTRACT

Numerical models of trajectories of small aerosol spheres relative to oblate spheroids were used to determine ice crystal scavenging efficiencies. The models included the effects of aerodynamic flow about the ice particle, gravity, aerosol particle inertia and drag and electrostatic effects. Two electric configurations of the ice particle were investigated in detail. The first applied a net charge to the ice particle, of magnitude equal to the mean thunderstorm charge distribution, while the second applied a charge distribution, with no net charge, to the ice particle to model the electric multipole charge distribution. The results show that growing ice crystals with electric multipoles are better scavengers than single ice crystals with net thunderstorm charges, especially in the Greenfield gap (0.1 to 1.0 μm), and that larger single crystals are better scavengers than smaller single crystals. The results also show that the low density ice crystals are more effective scavengers with net charges than they are with charge distribution.

I. INTRODUCTION

The problem of precipitation scavenging of atmospheric aerosols has drawn more and more attention in recent years due to the problem of acid deposition, also called acid rain. Scavenging by warm rain processes has been widely studied, both experimentally and theoretically. The question of ice crystal scavenging has been more difficult to answer, and the results more variable. In this article numerical models are used to determine ice crystal scavenging efficiencies as a function of their size, density and electric charge distribution.

Two theoretical models are formulated, which allows computing the efficiency with which aerosol particles of radii $0.05 < r < 60.0$ μm are collected by simple ice crystal plates. The hypothesis of electric multipoles, as well as their parameterized mathematical model, is given.

II. THE NUMERICAL MODELING OF ICE CRYSTAL SCAVENGING

1. *Background*

Basically, the ice particles presented in the atmosphere can be idealized as spheres, columnar disks or thin oblate spheroids. Jayaweera and Cottis (1960) and List and Schemenauer (1971) have experimentally demonstrated that the hydrodynamic drag on a thin disk is, within a small experimental error, the same as that on a simple hexagonal plate of the same radius. A similar result was obtained by Jayaweera (1972) from a comparison of the terminal fall speed of circular disks with simple hexagonal plates. The work of Pitter et al. (1973) also supported the hypothesis that simple hexagonal plates, disks and thin oblate spheroids have essentially the same flow fields, and consequently exhibit similar hydrodynamic

behavior.

Numerical solutions to the Navier–Stokes equations of motion were obtained by Michael (1966) for steady viscous flow past an infinitely thin disk with $1.5 < N_{Re} < 50$; and by Schlamp et al. (1975) for viscous flow around a columnar ice crystal employing the technique suggested by Hamielec and Raal (1969). Happel and Brenner (1965) discussed Stokes flow past an oblate spheroid on the basis of the work of Oberbeck (1876). Rimon (1969) and Rimon and Lugt (1969) obtained the numerical solution for time–dependent flow past oblate spheroids of axis ratio 0.05 and 0.2 and $N_{Re} = 10$, 100. Masliyah and Epstein (1970) studied the steady flow past oblate spheroids of axis ratio 0.2 and 0.5 and $N_{Re} = 1$, 5, 10, 20, 100. By pointing out the deficiencies of previous studies on solutions of flow past an oblate spheroid, Pitter et al. (1973) obtained numerical solutions of the full, steady–state Navier–Stokes equations of motion for the case of viscous flow past oblate spheroids of axis ratio lower than 0.2 and for a wider range of Reynolds numbers ($1 < N_{Re} < 50$). They adapted the numerical method employed by Woo (1971) for flow fields around spheres.

The present study is essentially an adaption to the last work. The flow fields used are based on those of Pitter et al., but differ from them in some details concerning the modification of streamfunction and interpolation of velocity field. These flow fields were employed for the study of ice crystal scavenging aerosol at intermediate Reynolds numbers ($N_{Re} = 2$, 5, 10, 20).

(1) *The calculation of the streamfunction*

The streamfunctions obtained by Pitter et al. (1973) were available for the present study. These data had been written to magnetic tape in E–format for archival. However, inspection of the variations of streamfunctions in the vicinity of the oblate body and close to the axis of symmetry yielded several regions where the streamfunction was not smooth. This fact may be attributed, in part, to the effect that at low Reynolds numbers considerable difficulties in the numerical calculation arise due to step size and wall effect. As a result, the application of finite–difference formulae for the velocity components would result in air flow velocity discontinuities, an unrealistic situation at intermediate Reynolds numbers. In an attempt to obtain accurate flow fields, a method for interpolation and curve fitting suggested by Stark (1970) was employed to smooth the streamfunction fields.

When analyzing the numerical solutions of Navier–Stokes equations of motion, it is instructive to examine the streamfunction at a given upstream grid point according to the following criteria:

$$\psi(I,J) \leqslant \psi(I+1,J), \qquad \psi(I,J) \leqslant \psi(I,J+1),$$
$$\psi(1,J) = 0, \qquad \psi(I,1) = 0,$$

where the index, I, represents the polar angle η and the second index, J, represents the radial coordinate ξ.

The interpolation was made along both polar and radial directions. An interpolating polynomial of $m-1$ order ($m = 8$ for the present study) was utilized:

$$P(X) = a_0 + a_1 X^1 + a_2 X^2 + \cdots + a_{m-2} X^{m-2} + a_{m-1} X^{m-1}, \tag{1}$$

where X could be either the polar or radial index, and coefficients $a_0, a_1 \cdots, a_{m-1}$ were computed by least square fit through grid points satisfying above criteria. The resulting interpolation function was therefore used to estimate the streamfunction at those discontinuous grid points.

This simple treatment for smoothing the streamfunction is believed to be crucial to the computational accuracy of the velocity field.

Figure 1 reveals the modified streamfunction for $N_{Re} = 2$. A 6° increment for the polar angle was adopted. The value for the radial coordinate increment was set at 0.1. The numbers in Fig.1 denote the radial coordinates. At the surface of the oblate spheroid, $\xi = \xi_0$, and $J = 1$, and at the outer boundary, $\xi = \xi_\infty$, and $J = 49$.

(2) *The interpolation of velocity fields*

As mentioned in the previous section, the velocity field generated by a falling oblate spheroid should tend to be undisturbed when approaching the outer boundary. Unfortunately, the theoretical results for velocity fields by Pitter et al. exhibited some negative values for z velocity components at grid points close to outer boundary. In order to resolve this deviation from the actual flow, a linear interpolation was used to modify the velocity fields. The expression for the vertical velocity components given by the flow field suggested that it may be in close proximity to assume a hyperbolic tangent for the interpolating function,

$$P(X) = a_0 + a_1 \operatorname{tgh} X \ , \tag{2}$$

where the coefficients a_0 and a_1 are again determined by least square fitting through those correct inner grid points and the outer boundary with zero velocity.

Considering the actual need for the determination of the collision efficiency in the later section, only the velocity in a narrow, far–upstream region was modified, of which the horizontal separation from the axis of symmetry was less than the semi–major axis length of the oblate spheroid.

2. *The Hypothesis of Electric Multipole*

In 1950, Workman and Reynolds investigated the electrical phenomena occurring during the freezing of dilute aqueous solutions, in an attempt to explain the mechanism of thunderstorm electricity. Their results, which have been termed the Workman–Reynolds effect, consist of electrostatic potential differences across the ice–water interface that arises during freezing of water containing low concentrations of ionizable salts, as a consequence of differential incorporation of anions and cations into the ice crystal lattice.

This theory has been substantiated and extended by experimental (Reynolds et al., 1957; Brook, 1959) and theoretical (Gross, 1954; LeFebre, 1967) work on charge transfer mechanisms, the effects of specific solutions (Gill and Alfrey, 1952; Gill, 1953; Lodge et al., 1956; Heinmets, 1962; Parreira and Eydt, 1965; Levi and Milman, 1966), the effect of electrode materials and electrode treatment on the charge separation (Carlin, 1956), the correction between freezing rate and preferential ion incorporation (Gross, 1965), solution partition coefficients (Gross, 1967) and spontaneous freezing of suppercooled solutions (Pruppacher et al., 1968). These electric effects have also been discussed by Gross (1968) and Cobb and Gross (1969).

Based on the interpretation of the Workman–Reynolds effect applied to atmospheric ice crystals, Finnegan and Pitter (1988) explained the aggregate of two single crystals and the resulting T–shaped crystals observed by Cheng (1967), Odencrantz (1968), Smith–Johannsen (1969) and Magono and Tazawa (1972).

They suggested that when water vapor condenses onto the ice crystal, the arriving water substance is initially in the transitory liquid phase, and as water becomes more ice–like, the water molecules in the surface layer are associated with bent and broken hydrogen bonds de-

pending on supersaturation and ice crystal temperature. Additionally, a number of ions are present, including ionizable species (salts) and water itself.

When the ice crystal is growing by vapor diffusion, the surface layer of water molecules undergoes ordered motion toward the growing ice crystal edge. Some ions, depending on the ionic species, are rapidly incorporated into the ice crystal lattice, while other ions are transported in the surface layer. Furthermore, there are ionizable molecules present, which may dissociate adding ions to the surface. As a result, there develops in many cases an electric multipole with two charges of opposite signs between the growing edge and the central area of the ice crystal.

However, this electric multipole can only exist while ice crystal is growing. When growth stops, the migration of ions will be sufficient to collapse the multipole.

The concept of quasi-liquid layer of ice is well established (Kuroda and Lacmann, 1982; Kuroda, 1982). On the surface of ice crystals near 0°C, various observational techniques verify its existence. Stickel (1982) has shown that the surface layer exists and affects aggregation of ice crystals down to at least −50°C.

Laboratory studies by Finnegan and Pitter (1988) have conclusively demonstrated that the effects of differential incorporation of ionic substances into the ice crystal lattice give rise to the electric multipoles in the growing ice crystals. Their results indicated a consistent pattern in the orientations of ice crystals in aggregates. They noted that, for distilled, deionized water cases, the predominant configuration was point-to-point junctions. For sodium chloride solutions, there was an increase in the proportion of T-shaped aggregates. When ammonium sulfate solutions were used, the T-shaped aggregates became the most frequently observed junction configuration. Their results of ice crystal collection on the charged wire with solutes present, which always showed ice crystal collection on the positive wires when ammonium salts were used to generate the cloud, and on the negative wires when sodium chloride was used, also supported the postulate of electric multipoles in growing ice crystals.

The Yellowstone Experiment (Cheng, 1967), when reanalyzed, provided additional evidence for the importance of dissolved salts in the orientation of initial ice crystal aggregates. The appearance of more T-shaped aggregates when silver iodide nuclei (2AgI-NaI) were used, as opposed to when dry ice was used for nucleation, indicated that something about silver iodide / sodium iodide acted such that the initial aggregates were strongly oriented point-to-center.

However, the work of Finnegan and Pitter does not answer the questions that concern the magnitude of the electric multipoles in growing ice crystals, and how strong the resulting electric fields are, since it was extremely difficult to conduct direct measurements.They attributed such difficulty to the nature of the electric multipoles, namely, that they only exist in growing ice crystals, and that the resulting electric fields are highly localized.

3. *Analytical Derivation of Electric Fields*

According to Finnegan and Pitter, the central area of the ice crystal possesses a net charge of one sign, and the growing edges possess a net charge of the opposite sign and equal magnitude, as a result of the developed electric multipole. We attempt to formulate this concept by allowing specification of two opposite charges on the ice crystal. One part, the polarity depending on the chemical ions present in the ice particle, is distributed on the crystal surface to make the surface a constant potential. This virtually results in a charge distribution such that most ions are present at the edges or tips of the crystal, due to the fact that the ice crystal has been idealized by an oblate spheroid of axis ratio 0.05. The other part, of equal

magnitude and opposite polarity, is characterized as a point charge at the center of mass of the ice crystal. Consequently, the electric behavior of the above physical model can be solved mathematically.

The electric field due to surface charge satisfies the condition,

$$E_1 = -\nabla\Phi_c, \tag{3}$$

where Φ_c is the potential around the ice crystal. Taking this potential to be zero far from the crystal, and assuming no background electric field from electric charges outside the ice spheroid, the electric potential satisfies Laplace's equation,

$$\nabla^2\Phi_c = 0. \tag{4}$$

The boundary conditions are given by the followings: on the surface of the spheroid,

$$\xi = \xi_o:\ \Phi_c = \Phi_o = \text{const}\ , \tag{5}$$

and at infinity,

$$\xi = \xi_\infty:\ \Phi_c = 0. \tag{6}$$

In oblate spheroidal coordinates, ξ and η, Eq.(4) has a particular solution,

$$\Phi_c = c_1 \sin^{-1}(\text{tgh}\xi) + c_2, \tag{7}$$

where the constants c_1 and c_2 are obtained from the boundary conditions,

$$c_1 = -\Phi_o[\pi/2 - \sin^{-1}(b/a_c)]^{-1}, \tag{8}$$

$$c_2 = (\pi/2)\Phi_o[\pi/2 - \sin^{-1}(b/a_c)]^{-1}. \tag{9}$$

From electrostatic theory,

$$\Phi_o = Q_c / C, \tag{10}$$

where the capacity C for a thin oblate spheroid is given by the relation (see Pruppacher and Klett, 1978),

$$C = \frac{a_c[1-(b/a_c)^2]^{1/2}}{\sin^{-1}\{[1-(b/a_c)^2]^{1/2}\}}\ . \tag{11}$$

Therefore, the electrostatic potential on any ξ surface in the space due to the charge distribution on the crystal surface is

$$\Phi_c = \frac{Q_c}{C}\frac{[\pi/2 - \sin^{-1}(\text{tgh}\xi)]}{[\pi/2 - \sin^{-1}(b/a_c)]}\ . \tag{12}$$

Considering Eq.(3), the electric field is

$$E_1 = -\frac{Q_c\,\text{sech}\xi}{a_c^2[1-(b/a_c)^2][\sinh^2\xi + \cos^2\eta]^{1/2}C[\pi/2 - \sin^{-1}(b/a_c)]}\ e\xi \tag{13}$$

where $e\xi$ is the unit vector in the ξ direction.

The separated charge Q_c on a growing ice crystal is expressed as,

$$Q_c = (4/3)\pi a_c^2 b(\rho/\rho_o)N_a R_e C_n, \tag{14}$$

where ρ_o is the density of ice at 0°C, and N_a is Avogadro's constant. The studies of freezing potential (Workman and Reynolds, 1950; Gross, 1968; Cobb and Gross, 1969) have measured the incorporation rate R_e for chloride ion into ice, and have found that it is approximately 2 part ions in 10^5 parts of water. C_n is a neutralization factor representing the balance between the incorporation rate of ions and the rate of charge migration or recombination, since ice behaves as a protonic semiconductor (Hobbs, 1974).

The electric field around an ice crystal generated by a point charge at the center of mass of the spheroid can be given in spherical coordinates as,

$$E_2 = \frac{Q_c}{r_s^2} e_r , \tag{15}$$

where e_r is the unit vector in the radial direction, and r_s is the center–to–center distance between the aerosol particle and ice crystal.

Finally, the superposition of the above formulated terms yields a reasonable reproduction of the electric field due to the electric multipole,

$$E_c = E_1 + E_2 . \tag{16}$$

4. *The Mathematical Models*

The trajectories of hydrodynamically interacting particles can be computed based on approximate formulations for the equations of motion. This method is frequently characterized by what is known as the superposition scheme, according to which each body is assumed to move in a flow field generated by the other falling in isolation.

Langmuir (1948), Shafrir and Neiburger (1963), Neiburger (1967), and Shafrir and Gal–Chen (1971) have successfully used the superposition method to compute the collision efficiencies of water drops. Beard and Grover (1974) and Grover and Beard (1975) similarly investigated aerosol scavenging by water droplets.

Investigations of ice crystal accretion have been conducted using the superposition method and nonspherical collecting bodies. Pitter and Pruppacher (1974), Pitter (1977) and Martin et al. (1981) studied riming by thin ice crystals, idealized by oblate spheroids of axis ratio 0.05. Schlamp et al. (1975) examined riming of ice columns and needles, idealized as circular cylinders.

Recent studies by Wang and Pruppacher (1980), Wang (1985) and Miller and Wang (1989) used an analytical flux model to investigate the scavenging of submicron aerosol particles by snowfall. This model considered the convective diffusion of aerosol particles less than 0.5 μm near an ice crystal and computed the particle flux by solving a steady–state ventilation–enhanced convective–diffusion equation. The mechanisms considered included Brownian diffusion, thermo– and diffusio– phoresis as well as electrostatic forces. Effects due to gravitation and inertial impaction were ignored for small aerosol particles.

The present study incorporates some features contained in the above two types of models. Two complimentary models which compute scavenging efficiencies by ice crystals have been formulated: 1) a trajectory model based on the superposition method for aerosol particle sizes 1 μm and larger and 2) a drift velocity model for aerosol particle sizes smaller than 1 μm. The combined trajectory and drift model therefore yields the scavenging efficiencies of aerosol particles of radii 0.05 to 10 μm by ice crystals.

(1). *Definitions and Relations*

The collision efficiency E is defined as

$$E(r,a_c)=\frac{\pi r_c^2}{\pi(a_c+r)^2}, \tag{17}$$

where r_c, measured perpendicular to the crystal fall axis aligned along g and sufficiently far upstream of the crystal, is the largest horizontal offset a particle can have from the ice crystal fall axis and still collide with the spheroid. In nondimensional form, Eq.(17) becomes

$$E(r,a_c)=Y_c^2/(1+P)^2, \tag{18}$$

where $p=r/a_c$ is the size ratio between the aerosol particle and ice crystal, and $Y_c=r_c/a_c$. Pitter and Pruppacher (1974) noted the noncollisionfree region could be expressed by

$$Y_{\min}<Y<Y_c,$$

where $Y_{\min}$ denoted the inner critical offset. Thus, we can employ a more complete relation to express the collision efficiency,

$$E(r,a_c)=(Y_c^2-Y_{\min}^2)/(1+P)^2. \tag{19}$$

The collision kernel $K(r,a_c)$, which is the effective volume swept by the scavenging body, can be computed from a knowledge of $E(r,a_c)$ and the following equation,

$$K(r,a_c)=E(r,a_c)\pi(a_c+r)^2(U_c-U_r), \tag{20}$$

where U_c and U_r are the terminal velocities of the collector crystal and of the aerosol particle, respectively.

It is reasonable to assume that adhesive forces ensure that a particle remains at the surface of an ice crystal once it has collided with it. This assumption is particularly justified at temperatures between 0 and −10°C, at which temperature water molecules have an appreciable surface mobility and behave as if being part of a "pseudo-liquid" layer. It also follows from Finnegan and Pitter (1988) that a liquid-like layer is required to dissolve salts and initiate electric multipoles in growing ice crystals, as noted earlier. With this assumption, the collision efficiency is then identical with the collection efficiency, and the collision kernel is identical with the collection kernel.

The scavenging coefficient $\wedge$, which is the loss rate of aerosol particles per unit volume of air by virtue of scavenging, is defined by the relation,

$$\wedge=-(1/n)(dn/dt), \tag{21}$$

where n is the number concentration of aerosol particles. The scavenging coefficient is also related to the scavenging kernel by the equation,

$$\wedge=\int_0^{\infty}K(r,a_c)N(D_c)dD_c, \tag{22}$$

where $N(D_c)$ is the differential number concentration of ice crystals with equivalent diameter between D_c and D_c+dD_c. For a given precipitation rate, R, and an ice crystal size distribution, the ice crystal number concentration can be solved from the relation,

$$R = (\pi / 6)\int_0^{\infty} D_c^3 U_c(D_c) N(D_c) dD_c . \tag{23}$$

The scavenging problem is therefore basically one of determining the collection kernel $K(r,a_c)$. For a monodisperse ice crystal size distribution of one crystal habit, one can have the simple result that,

$$\wedge = K(r,a_c)N(D_c) . \tag{24}$$

(2). *The trajectory model*

Particle trajectory models are based on Newton's second law of motion. Essentially, a trajectory model involves numerical integration of the equations of motion to determine the trajectory of the aerosol particle relative to ice crystal. The equation of motion for the aerosol particles is written as

$$m_r dV / dt = F_g + F_d + F_e , \tag{25}$$

where $m_r = (4 / 3)\pi r^3 \rho r$ is the mass of aerosol particle, F_g is the buoyancy– corrected gravitational force,

$$F_g = m_r g(\rho_r - \rho_a) / \rho_r , \tag{26}$$

where g is the gravitational acceleration, ρ_r is the bulk density of the aerosol particle and ρ_a is the air density.

The drag force, F_d, is due to the flow resistance to a body's motion within it. The resistance to the inertia of an assumed spherical object is expressed as

$$F_d = -6\pi\eta_a r(V - U) / C_{sc} , \tag{27}$$

where η_a is the dynamic air viscosity, and U is air motion experienced by the aerosol particles determined by solving the full Navier–Stokes equations of motion for each ice crystal. The Stokes–Cunningham slip correction factor has been defined by Junge (1963) as $C_{sc} = 1.0 + \alpha K_n$, with $\alpha = 1.26 + 0.40\exp(-1.1 / K_n)$. The Knudsen number, $K_n = \lambda / r$ is the ratio of the free path length of molecules, λ, to the aerosol particle radius, r.

The electrostatic force, F_e, on a particle near the ice crystal is

$$F_e = Q_r E, \tag{28}$$

where E can be either the electric field generated by the crystal surface E_1, or the electric field due to electric multipole E_c, as discussed previously. Q_r is the charge on aerosol particles.

For aerosol particles, the equilibrium charges may be determined from theoretical consideration of an energy distribution according to Boltzmann's law or considerations of recombination coefficients. However, Junge (1963) reviewed these theories and noted the lack of sufficient information to verify them. Grover and Beard (1975) indicated that corona breakdown of a perfectly spherical particle in the atmosphere occurs for 10^{-6} statcoulombs of charge and that over 99.9% of 1 μm particles contain charges of magnitudes of less than 5×10^{-9} statcoulombs. Data compiled by Takahashi (1973) indicated that the aerosol particle charge may be represented as

$$Q_r = qr^2, \tag{29}$$

where Q_r is in e. s. u. and r is in cm. The constant q ranges from 0.2 to 2.0, with the latter corresponding to the mean value in thunderstorm conditions. In the present study, the aerosol particles were modeled with either one electronic charge or a net charge given in Eq.(29) with $q = 2.0$.

The equation of motion for aerosol particles can be further nondimensionalized by the relations (superscript * denotes dimensionless quantity),

$$V^* = V / U_c, \tag{30}$$

$$t^* = tU_c / a_c \ . \tag{31}$$

Therefore, Eq.(25) is written in nondimensional form as

$$dV / dt = [(\rho_r - \rho_a) / \rho_r] g^* / N_{Fr} - (V - U) / N_s + (3a_c) / (4r^3 \rho_r U_c^2) Q_r E, \tag{32}$$

where $N_{Fr} = U_c^2 / a_c g$ is the Froude number for the aerosol particle, g^* is a unit vector in the direction of gravity, and

$$N_s = (2r^2 \rho_r U_\infty / 9\eta_a a_c)(24 / C_D N_{Re}), \tag{33}$$

is the inertia parameter, or Stokes number for the ice crystal.

As formulated, Eq.(32) includes effects of inertial, gravitational, hydrodynamic and electrostatic forces on the trajectories of the aerosol particles. Although the nonlinear effects of two body interactions were not treated, this method has been found accurate when the axis ratio of the two particles is significantly less than unity (Grover, 1980). Furthermore, the flow fields around the aerosol particles have been omitted from this model since they have negligible effect on the crystal velocity.

(3) *The drift velocity model*

The drift velocity model is a simplification of the superposition model which is applicable to aerosol particles less than 1 μm radius. In Eq.(25) the aerosol particle acceleration arises from an imbalance of external forces. If the aerosol mass is extremely small, the acceleration becomes so large as to almost instantaneously balance the external forces. Mathematically, this can be achieved by setting the left–hand side of Eq.(25) to zero and solving for V,

$$V_d = U + (6\pi\eta_a r / C_{sc})^{-1}(F_g + F_e), \tag{34}$$

where V_d is known as the average response to the impressed forces, which is also termed as drift velocity.

The particle mobility is defined (see Pruppacher and Klett, 1978) as

$$B = C_{sc} / (6\pi\eta_a r) \ . \tag{35}$$

On combining Eqs.(34) and (35), we can obtain an intimate connection between the drift velocity and the particle mobility,

$$V_d = U + B(F_g + F_e) \ . \tag{36}$$

Similarily, this equation can be nondimensionlized by using Eq.(30),

$$V_d = U + (B / U_c)[(4 / 3)\pi r^3 (\rho_r - \rho_a) g^* + Q_r E] \ . \tag{37}$$

From the numerical solutions of Eqs.(32) and (37), the trajectory can be computed for aerosol particle of various sizes moving around the oblate spheriod of ice of various sizes.

Collision can occur as front or rear captures. Rear capture may occur when there are eddies present and when electrostatic forces exhibit weakly net attractive forces. When eddies are present, a collision is said to occur once an aerosol particle is trapped in a circulating eddy in the wake of the ice crystal. The value of Y_c is found by choosing an initial offset $Y_i = (Y_1 + Y_h)/2$ (Y_1 is initially zero, and Y_h is initially one ice crystal radius), and integrating in time for the resultant trajectory. The initial trajectory is chosen to always miss, and the subsequent initial offset is determined by bisecting the offset value, i.e., for a miss $Y_h = Y_i$, for a hit, $Y_1 = Y_i$, i is the particular iteration. A grazing collision occurs when $(Y_h - Y_1)/Y_i < c$, where $c = 10^{-4}$ is the collision tolerance.

In order to ensure that the vertical separation between the ice crystal and aerosol particle has a negligible effect on the collision efficiency, the initial vertical separation was chosen to be sufficiently large (15 ice crystal radii in the present study) such that any additional increase in initial vertical separation changes the collision efficiency by $<0.1\%$. This represents the situation as it is found in an atmospheric cloud free of turbulence (Martin et al., 1981).

It was found that the integration scheme used to solve Eqs.(32) and (37), and hence the collection efficiency, was very crucial to the accuracy and stability of the trajectories. As a result, it was determined to use Hamming's predictor–corrector–modifier method, a non–self–starting method, with the Runge–Kutta method to start the integration. Both the Hamming and Runge–Kutta schemes are of fourth–order accuracy, and both contain error controls. If the estimated error incurred in one step exceeded a specified value, the step size was halved, reducing the error by a factor of 32. If later the error was diminished significantly, the step size was doubled as feasible until it reach its initial size.

III. CASES INVESTIGATED

The present models were applied to a variety of cases to survey the effects of aerosol particle size and ice hydrometer density, size and charge on scavenging efficiency.

Essentially, two series of investigations were performed with ice crystals of different bulk densities. The first series investigated ice crystals of bulk density 0.92 g / cm^3 and Reynolds numbers 2, 5, 10, and 20. The second series investigated ice of bulk density 0.1 g / cm^3 and the same Reynolds numbers. The field studies of natural ice crystal by Locatelli and Hobbs (1974) indicated that the bulk density of 0.1 g / cm^3 is typically found in snowflake aggregates. Although the ice crystals considered in the present study are much smaller than those observed by Locatelli and Hobbs, the second series resembles the ice hydrometer behavior as it is to some extent for natural snowflakes. The first series, on the other hand, pertains to simple, unrimed and unaggregated ice particles.

For each of these cases, ice crystals were modeled for two electrostatic conditions. In the first, representing the net charge case, they were assigned a net electric charge as given by Eq.(29), with the surface charge distributed so as to make the surface equipotential. In the second, representing the electric multipole case, there is no net charge, but two components of equal magnitude and opposite sign, with an internal charge distribution as specified in section 2.3. In order to visualize the importance of the strength of electric multipole on the aerosol scavenging, it is useful to examine the trajectories of aerosol particles relative to ice crystal at different ionic charge neutralization. In the present study, the collision efficiency was comput for ionic charge neutralizations of 99.9% and 99.99%.

The present study was not oriented toward investigating in detail the nature of scavenging for aerosol particles greater then 10 μm, since the electric forces have a negligible effect on

scavenging efficiency for such large aerosol particles. However, a limited number of investigations were conducted to examine the effect of net electric charges on the efficiency with which aerosol particles of radii larger than 10 μm are collected by ice crystals, with the intention to examine the validation of the present model and to compare it with published models.

Model I was evaluated for platelike ice crystal of bulk density 0.92 g / cm^3. The aerosol particles considered have radii of $1.0<r<60.0$ μm. The ice crystal plates have Reynolds numbers of 5, 10, and 20. In addition, the present study also investigated the interaction of uncharged aerosol particles and ice hydrometers for comparison.

In all cases, ice crystals are represented as oblate spheroids of axis ratio 0.05. The aerosol particles considered to be spheres with a bulk density of 1.0 g / cm^3. The ice crystals were assumed to fall at the atmospheric environmental conditions of −10°C and 700 hPa.

In order to obtain the aerosol particle trajectories, it is necessary to know the drag coefficient C_D for the ice crystals. The results for oblate spheroids were those numerically determined by Pitter et al. (1973). It is also necessary to know the size and terminal velocity of an oblate spheroid of given Reynolds number and drag coefficient. These results can be derived from the vertical component of Eq. (25) for the case of an oblate spheroid falling at terminal velocity in an infinite, undisturbed environment, and only including buoyancy mentioned previously

$$a_c = [3v_a^2 C_D N_{Re}^2 / 32gAR(\rho_c - \rho_a)\rho_a]^{1/3}, \tag{38}$$

$$U_c = v_a N_{Re} / (2a_c \rho a) . \tag{39}$$

Table 1 relates the Reynolds number N_{Re}, drag coefficient C_D, radius a_c and terminal velocity U_c of oblate spheroid of density of 0.92 g / cm^3 in atmosphere of −10°C, 700 hPa.

Table 1. Reynolds Number, Drag Coefficient, Radius and Terminal Velocity for Simple Ice Crystal Plates of Density of 0.92 g / cm^3 in Atmosphere of −10°C and 700 hPa

Reynolds number N_{Re}	Drag coefficient C_D	Crystal radius a_c (μm)	Terminal velocity U_c (cm / s)
2	12.67	147	12.25
5	6.17	213	21.14
10	3.87	289	31.11
20	2.63	404	44.59

Table 2. Comparison between Computed and Observed Terminal Velocities of Simple Ice Crystal Plates

Crystal radius a_c (μm)	Terminal velocity computed for oblate spheroids of ice of $(b / a_c) = 0.05$ 700 hPa, −10°C (cm / s)	Terminal velocity observed for simple hexagonal ice crystals (Kajikawa, 1972) 1000 hPa, −10°C (± 3 cm / s)
147	12.25	12
213	21.14	21
289	31.11	30
404	44.59	42

In Table 2, comparison is made between the theoretically predicted fall velocity, available for 700 hPa and −10°C, and the fall velocity experimentally measured by Kajikawa (1972) for 1000 hPa and −10°C. Considering the difference in pressure, the two data sets appear to be in good agreement and thus justify further our idealization of simple hexagonal ice crystal plates by thin oblate spheroid of ice.

The net electric charge of ice crystals computed from Eq.(29) and the separated charge given by Eq.(14) for electric multipole without neutralization are listed as functions of ice crystal sizes in Table 3. It appears from field observations (Magono and Kikuchi, 1961; Isono et al., 1966; Burrows and Hobbs, 1970; Kikuchi, 1973; and Magono and Iwabuchi, 1979) that platelike crystals are predominantly negatively charged. In contrast, in partially glaciated clouds, the aerosol particles may carry either positive or negative electric charges. However, in the present study, only collisional interactions between an ice crystal and aerosol particle of opposite charge sign are considered. Due to the strongly opposing electric forces, it is obvious that the collision efficiency for ice crystals and aerosol particles of like charge sign is very small. Similarly, only the case with opposite charge signs between that of the aerosol particle and that of surface charge on the ice crystal arising from the internal charge distribution is evaluated in this study.

Table 3. Net Electric Charge and Computed Growing Crystal Charge Separation due to Electric Multipole for Simple Ice Crystal Plates of Bulk Density 0.92 g / cm^3

Crystal radius a_c (μm)	Computed charge separation (esu)	Net crystal charge (esu)
147	3.85	-4.3×10^{-4}
213	11.70	-9.1×10^{-4}
289	29.26	-1.7×10^{-3}
404	79.80	-3.3×10^{-3}

Table 4. Reynolds Number, Drag Coefficient, Radius and Terminal Velocity for Simple Ice Crystal Plates of Density of 0.1 g / cm^3 in Atmosphere of −10°C and 700 hPa

Reynolds number N_{Re}	Drag coefficient C_D	Crystal radius a_c (μm)	Terminal velocity U_0 (cm / s)
2	12.67	310	5.83
5	6.17	449	10.07
10	3.87	610	14.83
20	2.63	852	21.14

Table 5. Net Electric Charge and Computed Growing Crystal Charge Separation due to Electric Multipole for Simple Ice Crystal Plates of Bulk Density 0.1 g / cm^3

Crystal radius a_c (μm)	Computed charge separation (esu)	Net crystal charge (esu)
310	3.92	-1.92×10^{-3}
449	11.92	-4.03×10^{-3}
610	29.91	-7.45×10^{-3}
852	81.33	-1.45×10^{-2}

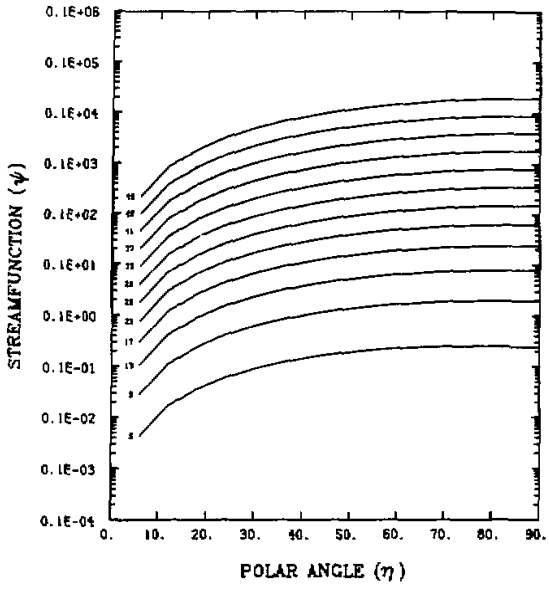

Fig.1. Modified streamfunction versus polar angle for ice crystal Reynolds number $Re = 2$. The numbers correspond to radial distances to the spheroidal surface.

IV. RESULTS AND DISCUSSIONS

1. *Simple Ice Crystal Scavenging*

(1) *Thunderstorm ice crystal scavenging*

Figure 2 presents the results for the efficiency with which electrically charged simple ice crystal plates and oppositely charged aerosol particles collide with each other, along with the results for the efficiency with which uncharged simple ice crystal plates collide with uncharged aerosol particles, in air at 700 hPa and −10°C. These results were obtained by evaluating model I for aerosol particles of radius $1 \leqslant r \leqslant 60$ μm. Ice crystal Reynolds numbers of 5, 10 and 20, corresponding ice crystal sizes of 213, 289 and 404 μm, were investigated. The dotted lines identify results for attractive electrostatic force cases. Solid lines denote the numerical results for uncharged bodies.

It is seen from Fig.2 that, for electrically uncharged aerosol particles and crystals, the collision efficiency rapidly increases with increasing aerosol size up to a broad maximum beyond which the collision efficiency rapidly decreases to zero. It is noted that there exist a small aerosol size cutoff and a large aerosol size cutoff for uncharged bodies, dependent on the ice crystal Reynolds number investigated. For Reynolds number of 10 as an example, the cutoffs are located at 6 and 46 μm. These cutoffs were also previously noted by Pitter and Pruppacher (1974) and Martin et al. (1981). The small aerosol size cutoff is due to the fact that a small aerosol particle has little inertia and tends to escape being captured by following the streamline. This has been verified by the field observations of Wilkins and Auer (1970),

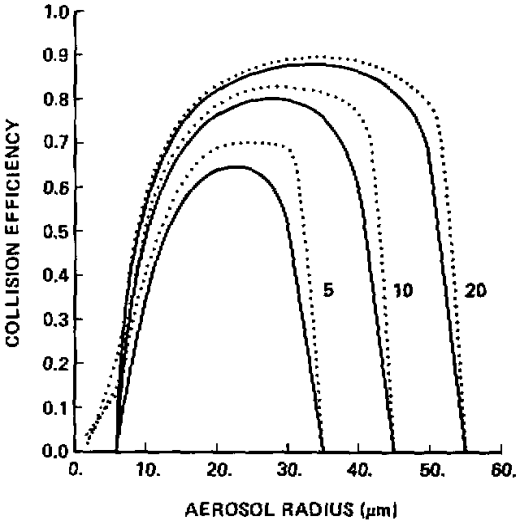

Fig.2. Collision efficiency with a simple ice crystal plate of bulk density 0.92 g / cm^3 and a given Reynolds number collides with an aerosol particle of given size, for the case of electrically charges (dotted lines) and uncharged (solid lines) ice crystals and aerosol particles at 700 hPa and −10°C. The numbers denote ice crystal Reynolds numbers.

Harimaya (1975) and Kikuchi and Uyeda (1979), who found that drops smaller than 5 μm are rarely found on rimed ice crystal plates collected in natural clouds. The large aerosol size cutoff is due to the combined action of hydrodynamic forces, viscous drag and gravitation settling. The large aerosol particles accelerate to the terminal velocity of the ice crystal plates, thus allowing the long interaction time so that the aerosol particle can accelerate and subsequently cross streamline away from the ice crystal by virtue of its drag force.

The present results indicate that electrostatic charges on ice particles in convective clouds increase the collision efficiency over that for uncharged case, when oppositely charged aerosol particles and ice crystals interact. Such electrical effect on ice crystal scavenging is particularly notable for ice crystals of smaller Reynolds numbers, which have smaller collecting areas and low terminal velocities.

When attractive electric forces are considered, the small aerosol size cutoff vanishes for all cases investigated. Essentially, small aerosol particles are able to accelerate towards the ice crystal because of the electric forces. However, the action of electric field does not noticeably affect the large aerosol cutoff size, since large aerosol particles have greater inertia and thus smaller acceleration due to the electric forces.

A comparison of the present results for interaction between uncharged and charged bodies with the results previously computed by Martin et al. (1981) shows slight differences both in the collision efficiency and in the aerosol size cutoff. For all cases investigated, the collision efficiencies presented in this study are somewhat lower than the results of Martin et al. This difference may be attributed to the different collision criteria or to the different vertical separations specified in each study. The initial vertical separation used in this study is considerably larger than that of Martin et al., and as a result, the collection efficiency is more representive of an aerosol particle approaching from infinity.

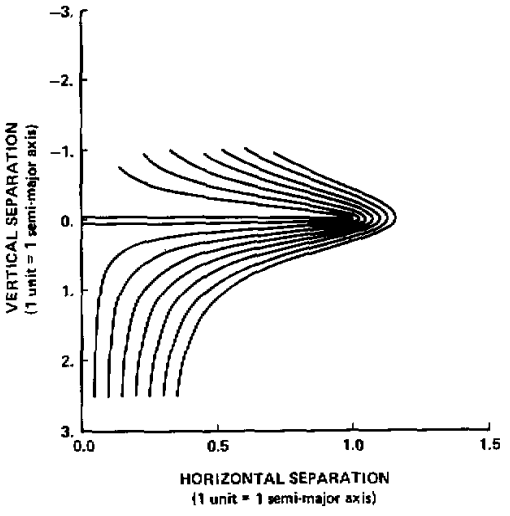

Fig.3. 0.1 μm aerosol trajectories about an ice crystal with $N_{Re} = 2$ for the case of uncharged bodies.

Furthermore, in contrast to the studies of Martin et al., who showed that sufficiently small, electrically charged aerosol particles may be only captured in the front of electrically charged ice crystal plates, the present study indicates that, for the aerosol and crystal sizes considered, both front and rear captures of aerosol particles take place.

Figure 3 shows trajectories that 0.1 μm aerosol particles move about an ice crystal with Reynolds number $N_{Re} = 2$ for the case of uncharged bodies. It is noted that inertial impaction is negligible for such small aerosol particles.

The results for interaction between electrically charged ice crystals and electrically charged aerosol particles of radius less than 10 μm are shown in Figure 4, by evaluating model I and II for ice crystal Reynolds number 2, 5, 10 and 20. In this figure gravitational, diffusive, and electrical forces are considered. Two regimes are readily apparent in this figure. The first, for $r \leqslant 0.3$ μm, is characterized by decreasing scavenging efficiency with increasing aerosol size. The second, for $r > 0.3$ μm, is characterized by the opposite behavior. The decrease in efficiency with increasing aerosol size for $r \leqslant 0.3$ μm is due to the fact that the dirft velocity (i.e., mobility) of smaller aerosol particles in the electric field is much larger than that of large aerosol particles, thus allowing the smaller aerosol particles to experience larger average deviations from the streamlines, and consequently increasing the probability of collision with the ice crystal. In this case, as the aerosol size increases, the corresponding particle mobility, B, decreases, while the aerosol particle charge remains one electron. The observed increase in efficiency with increasing aerosol particle size for $r > 0.3$ μm is due to the fact that the aerosol particle charge is specified to be size-dependent as given in Eq.(29), and due to the increasing role of inertial impaction.

Figure 4 also shows that, for aerosol particles smaller than about 6 μm, the collision efficiency increases as the ice crystal Reynolds number (i.e., the size of the collector) decreases. This increase is particularly noticeable for aerosol particles near 0.03 μm. Since aerosol

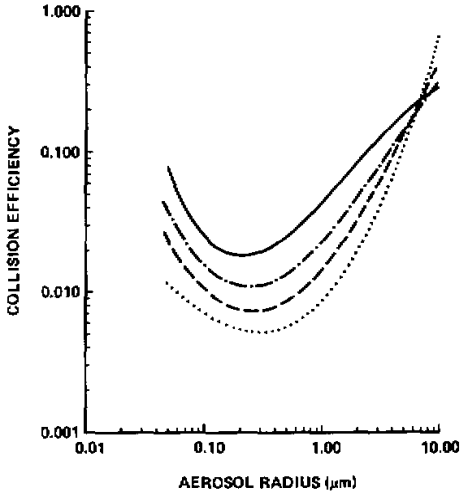

Fig.4. Collision efficiency with which a simple ice crystal plate of bulk density 0.92 g / cm^3 and a given Reynolds number collides with an aerosol particle less than 10 μm for the case of electrically charged ice crystals and aerosol particles. Solid line: $N_{Re} = 2$; Dot–dashed line: $N_{Re} = 5$; dashed line: $N_{Re} = 10$; dotted line: $N_{Re} = 20$.

diffusive impaction dominates the collection process, and since the larger Reynolds number corresponds to larger ice crystal terminal velocity, thus allowing less time for interaction between the two particles, the above–mentioned behavior is expected.

The present results for submicron ice crystal scavenging with attracting electrical forces between the interacting bodies are consistent with the low scavenging efficiency obtained theoretically by Miller and Wang (1989), who took account of thermo– and diffusio–phoresis as well as electrostatic forces. We noticed that, at present, no published numerical studies are able to match those observed high scavenging efficiencies as indicated earlier. The strong net charges, what are considered to be the average charges on ice crystals in thunderstorms, were required for even modest collision efficiencies. In addition, some experimental data have shown that orographic winter storms were capable of vigorous scavenging, although such storms lacked the electrification that thunderstorms possess. Therefore, there might exist some other mechanisms which are effective for submicron ice crystal scavenging.

(2) *Aerosol scavenging by ice crystals due to electric multipoles*

Some calculations were performed to simulate the effect of internal charge distributions in ice crystals on scavenging of aerosol particles. It was assumed that there is no net charge on the ice crystal, but rather two components of charge of equal magnitude and opposite sign. One component was distributed on the crystal surface, in the same manner as an equipotential surface charge noted previously. The other was characterized as a point charge at the center of mass of crystal. The combination of Model I and II provides scavenging efficiencies for aerosol particles of radius $0.05 \leqslant r \leqslant 10.0$ μm by plate ice crystals with associated Reynolds numbers ranging from 2 to 20.

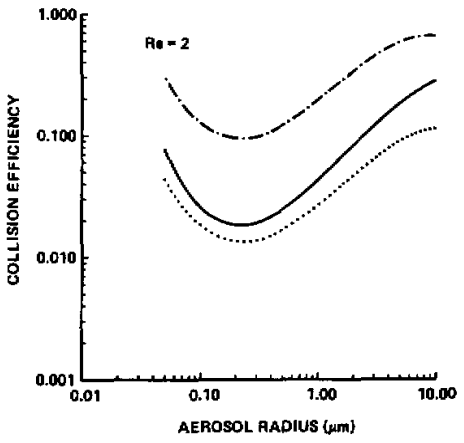

Fig.5. Collision for ice crystals of bulk density 0.92 g / cm^3 and $N_{Re} = 2$. Solid line: net charge model: dot–dashed line: eletrostatic multipole with 99.9% neutralization; dotted line: electrostatic multipole with 99.99% neutralization.

Figure 5 presents the scavenging efficiencies for ice crystals of Reynolds number 2, comparing the result of a net charge on crystal surface (solid line) with those arising from electric multipoles. The upper, dot–dashed curve is computed by assuming that chloride ions are incorporated into ice at 2 parts in 10^5 parts of water, and that 99.9% of the electric charge associated with the chloride ions are neutralized at any moment. The lower, dotted curve assumes the same, except that 99.9% of the electric charge associated with the chloride ions are neutralized. Similarly, Figs. 6 to 8 present the results for ice crystals of Reynolds numbers 5, 10, and 20, respectively.

Figs. 5 to 8 indicate that the presence of electric multipoles may significantly affect the capture of aerosol particles by ice crystals, particulary in the aerosol range of $0.1 \leqslant r \leqslant 1.0$ μm, namely, in the Greenfield Gap. For aerosol particles of $r > 1.0$ μm, the effects of electric multipoles are small because inertia dominates the capture process. For aerosol particles of $r \leqslant 0.1$ μm, the electric effects are small since the capture process is dominated by aerosol diffusion (i.e., extremely large particle mobility). It is seen that the smaller the size of ice crystal plate, i.e. the smaller the Reynolds number is and hence the less the strength of the flow field around the crystal becomes, the stronger the action of electric multipoles is. As the Reynolds number increases to 20, the charge distribution effect is minimal for aerosol particles larger than a few micrometer radii, but still strongly pronounced for submicron aerosol particles. The disappearance of the effects of electric multipoles for aerosol particles of $r > 10$ μm and ice crystal Reynolds number greater than 10 is not surprising, since the capture processes are completely dominated by inertia impaction for large ice crystals and large aerosol particles.

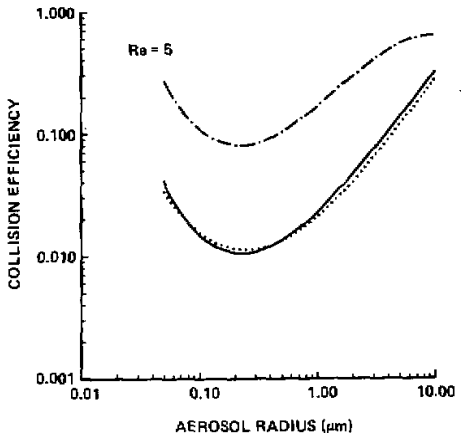

Fig.6. Same as Fig.5 except for ice crystal with $N_{Re} = 5$.

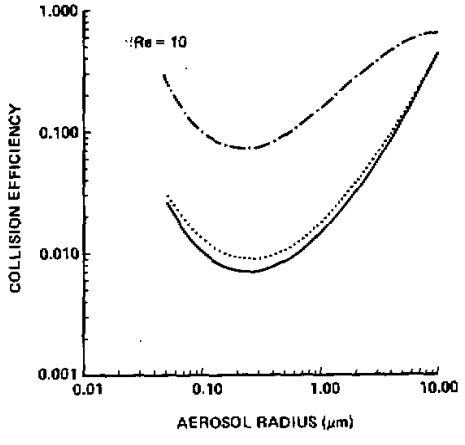

Fig.7. Same as Fig.5 except for ice crystal with $N_{Re} = 10$

Figs. 5 to 8 show that the strength of electric multipoles influences the efficiency with which aerosol particles collide with ice crystals. For aerosol particles of $0.1 \leqslant r \leqslant 1.0$ μm, a change from 99.99% to 99.9% of ionic charge neutralization causes an increase in the efficiency of about one order of magnitude. This implies that the scavenging effect may be strongly dependent on the crystal growth rate and on the concentrations and species of available ions presented in the crystal. Ice crystals growing rapidly by vapor diffusion are, therefore, able to act as efficient aerosol scavengers.

Figs.5 to 8 indicate that aerosol particles less than 1 μm are subject to increasing collision efficiencies for decreasing ice crystal N_{Re}, while aerosol particles greater than 2.0 μm exhibit the opposite behavior. Since smaller ice crystal Reynolds number means longer interaction time between aerosol particles and crystal hydrometers, and consequently the aerosol diffusion is more effective the smaller the collector, the above mentioned behavior is expected. The observed predominant minimum in the collision efficiency for aerosol particles of radius between 0.1 μm and 1.0 μm may occur as the combined effect of aerosol mobility and the sum of the radially directed forces (i.e., the gravitational and electric forces) approach minimum. This result is consistent with the "Greenfield gap", with the aerosol collision efficiency attaining its minimum value at around 0.2 μm in radius.

2. *Aerosol Scavenging by Low Density Ice Crystals*

Several calculations were carried out using a low density for ice particle. The crystal density was decreased from 0.92 g / cm^3 to 0.1 g / cm^3. Although the configuration of electrical multipoles in ice crystal aggregates may be more complicated than that of simple ice crystal plates, it was still assumed that the characteristics of electrical multipoles discussed in section 3.3 is hold true for the low density ice crystals. Models I and II were evaluated for ice crystal Reynolds numbers 2 to 20 and aerosol particle radii of $0.05 \leqslant r \leqslant 10.0$ μm.

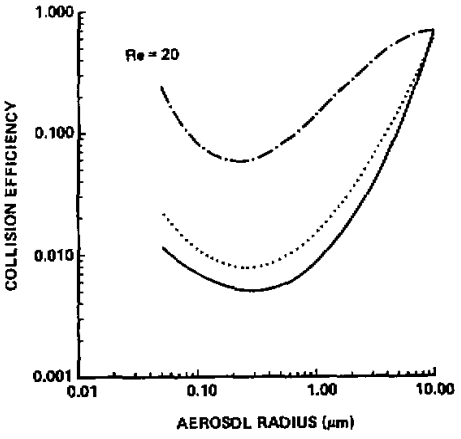

Fig.8. Same as Fig.5 except for ice crystal with $N_{Re} = 20$.

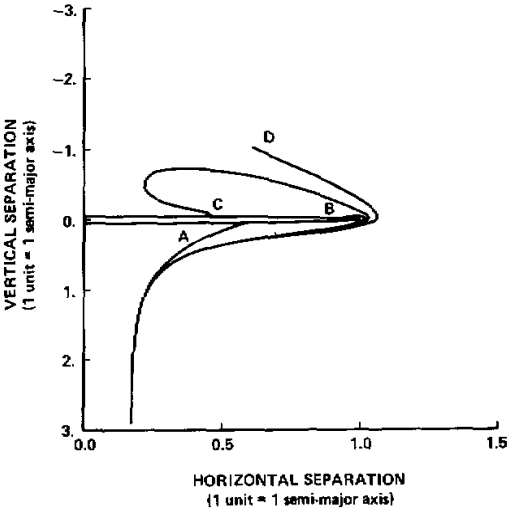

Fig.9. 0.05 μm aerosol trajectories about an ice crystal with $N_{Re} = 10$. Curve A: electric multipole with 99.9% charge neutralization; curve B: electric multipole with 99.99% charge neutralization; curve C: net charge model; curve D: no net charge model.

The strongly attracting effect due to electric multipole is also evident by the analysis of the aerosol trajectories during close interaction with the ice crystal. The different charge scenarios is portrayed by plotting the trajectories of four identical cases with different crystal charges. Figure 9 shows comparative trajectories for an 0.05 μm radius aerosol particle around an ice crystal of Reynolds number 10. The trajectory that yields no collisions is for uncharged ice crystal and aerosol particle, with only the inertial force involved. The trajectories with rear captures, the one close to the rim and the one far from the rim, indicating that they are very close to the critical trajectory, are for the electric multipole with 99.99% charge neutralization and the net charge case, respectively. The inner trajectory is for the case of an

internal charge distribution on the ice crystal with a 99.9% recombination factor. It yields capture of the aerosol particle on the front side of the ice crystal. From this direct comparison, it is seen that the existence of electric multipoles strongly affects aerosol particle trajectories in its immediate vicinity, and hence the scavenging efficiency. The cause of the dramatic deviation of the aerosol particle from its streamline for the case of electric multipoles must be attributed to the fact that the attracting force is strong enough to move the particle toward the crystal as the aersol particle approaches the crystal. In all cases, the aerosol particle was considered to have either no net char ge or one electron of charge.

Figure 10 presents various aerosol trajectories moving around an ice crystal for the case of electrical multipole and ionic recombination factor 99.99 percent. The ice crystal is 147 μm in radius (Reynolds number 2), while the aerosol radius is 0.1 μm. The trajectories were computed by specifying the initial horizontal aerosol offsets at equal intervals. It is noted that the distribution of captured aerosol particles are non-uniform on the crystal surface, with more aerosol particles captured close to the rim. This may be explained by the joint action of the deflected air flow beneath the ice crystal and the greater surface charge density at crystal edge. This result is consistent with the cloud chamber work of Prodi (1976) and the theoretical work by Martin et al. (1980).

Figure 11 explicitly illustrates the scavenging coefficient dependence on Reynolds number for the case of electric multipoles. The scavenging coefficient has units of inverse time, and represents the inverse of the time it takes the ice crystal population to reduce the aerosol concentration to 1 / e of its original concentration. The ice crystal number concentrations were assumed to be the same for all crystal sizes considered, thus allowing comparison of scavenging coefficients for various sizes of ice crystals. This ice crystal number concentration was derived by assuming that, at certain level, a precipitation rate of 1 mm / hr was caused by monodisperse ice crystals of radius 404 μm (Reynolds number 20). For all cases, the electric multipoles were considered with 99.9 percent charge recombination. It is seen that the existence of electric multipoles cause a rapid removal of aerosol particles from the atmosphere. For example, for Reynolds number 20 and aerosol size range of $0.05 \leqslant r \leqslant 10$ μm, the values of computed scavenging coefficients are $7 \times 10^{-4} < \Lambda < 8 \times 10^{-3}$ s^{-1}. As a result, the aerosol resident time due to snow scavenging is between 0.4 and 0.035 hours. The results show that larger ice crystals are more effective scavengers than smaller ice crystals, and that larger ice crystals are more effective scavengers, in term of scavenging coefficient, than liquid water drops. The higher scavenging effect for larger ice crystals can be attributed to the fact that the collecting area and terminal velocity increase as a result of increasing ice crystal size. It is also noted that for a given ice crystal size the variation of scavenging coefficient with aerosol size resembles that of scavenging efficiency.

The results from electrical multipoles with 99.9% and 99.99% charge recombination factors are compared with those from the net charge model. The most significant feature of the calculated results is that, for aerosol particle size larger than a few micrometers, the scavenging efficiences drop rapidly with increasing aerosol size for the electric multipoles with 99.99% neutralization, and subsquently approach zero, due to the lack of sufficient electrical action and small differential terminal velocities between the ice crystal and aerosol particle.

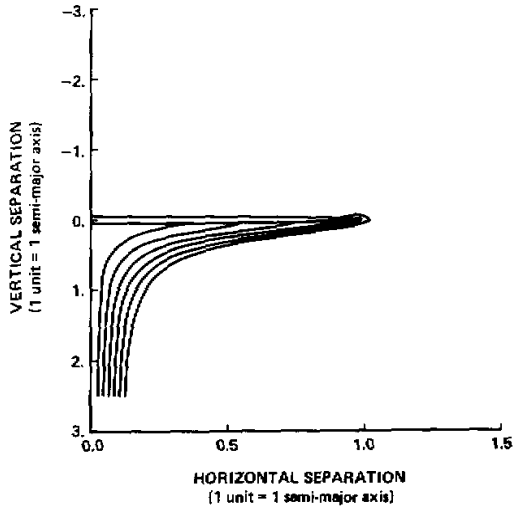

Fig.10. 0.1 μm aerosol trajectories about an ice crystal with $N_{Re} = 2$ for the case of electric multipoles with 99.99%charge neutralization.

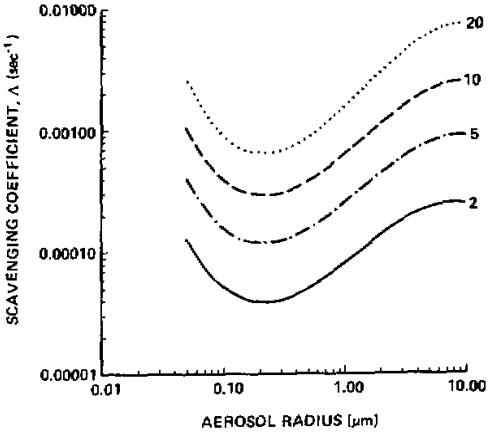

Fig.11. Scavenging coefficients for the case of electric multipole with 99.9% charge neutralization. Solid line: $N_{Re} = 2$; dot–dashed line: $N_{Re} = 5$; dashed line: $N_{Re} = 10$; dotted line: $N_{Re} = 20$.

A comparison of the aerosol scavenging efficiency by ice crystals of density 0.1 g / cm^3 with those of bulk density 0.92 g / cm^3 indicates that, for the case of electric multipoles, the low density crystals are less efficient scavengers than those of high density ice crystals, although the scavenging efficiency is still strongly pronounced for electric multipoles with 99.9% neutralization. It is also noted that, for all Reynolds numbers investigated, the effects of crystal net charges increase for low density ice crystals.

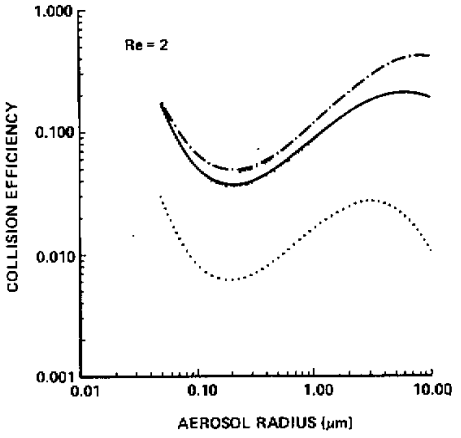

Fig.12. Collision efficiencies for ice crystals of bulk density 0.1 g / cm^3 and Reynolds number $N_{Re} = 2$. Solid line: net charge model; dot–dashed line: electrostatic multipole with 99.9% neutralization; dotted line: electrostatic multipole with 99.99% neutralization.

These findings can be interpreted as that the role of the ice crystal internal charge distribution in aerosol scavenging is primarily limited to scavenging by simple ice crystals. As aggregates form and grow, the charge distribution effect becomes minimal, while the net charge effect increases.

V. SUMMARY

A combined numerical model was developed and utilized to incorporate inertial, hydrodynamic, gravitational and electrostatic forces, including forces arising from an internal electric charge distribution in the ice crystals, to determine aerosol trajectories and scavenging by simple ice crystal plates and snowflakes.

Two numerical models were used. Scavenging of aerosol particles from 1 to 10 μm was studied using a trajectory model based on Newton's second law of motion. Scavenging of smaller aerosol particles was studied using drift velocity model based on the concept of particle mobility. A model to estimate the effects of electric multipoles, as postulated by Finnegan and Pitter (1988) was also developed to survey the effects that differential ion incorporation into the ice crystal lattice might have on scavenging efficiency.

In the modeled thunderstorm cases, the results of the numerical models indicate that, for larger aerosol particles ($r > 5$ μm), the effects of attractive electrostatic forces generally increase the crystal scavenging efficiency. It was found that inertial impaction is usually the dominant mechanism if the aerosol particle Stokes number exceeds a critical value. The action of combined electrostatic deposition and inertial impaction causes the small aerosol size cutoff to vanish. However, for submicron aerosol particles, particularly those in the region of $0.1 \leqslant r \leqslant 1.0$ μm, the net charge model yields only lower scavenging efficiencies.

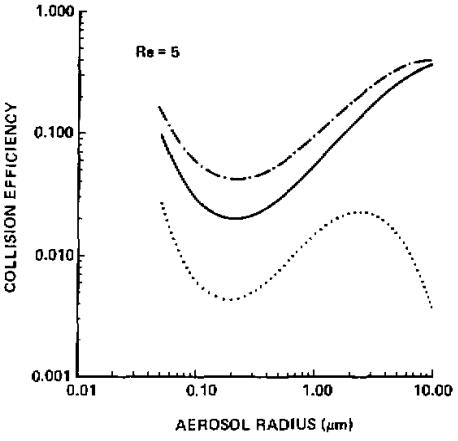

Fig.13. Same as Fig.12 except for ice crystal with $N_{Re} = 5$.

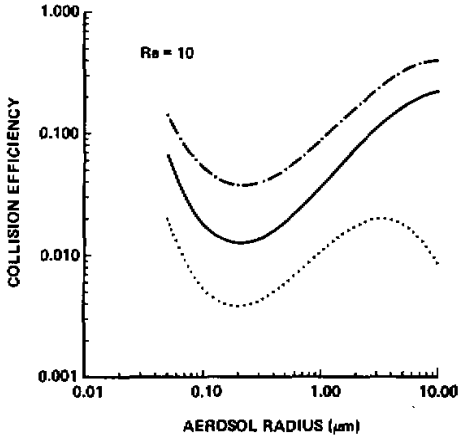

Fig.14. Same as Fig.12 except for ice crystal with $N_{Re} = 10$

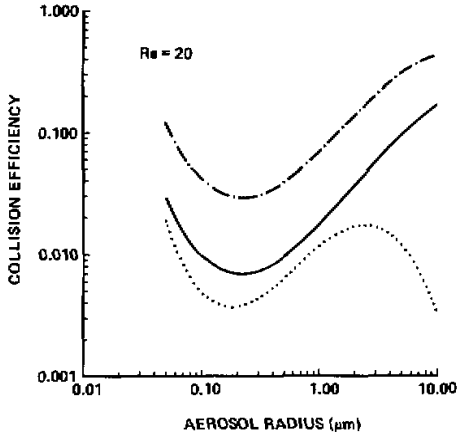

Fig.15. Same as Fig.12 except for ice crystal with $N_{Re} = 20$.

The numerical simulations of aerosol trajectories and scavenging by ice crystals with an internal charge distribution have shown remarkable ability to reconcile the previously widely diverging results of many investigators. The study suggested that the aerosol scavenging efficiency by snow crystals may depend on the ionic species present in ice crystals, their concentrations and ice crystal growth rates. The computations with stronger electrical multipoles, which are postulated to exist when ice crystals contain dilute concentrations of ionizable inorganic salts and are growing rapidly by vapor diffusion, yielded results consistent with higher scavenging efficiencies found experimentally, and heretofore unexplained mechanistically. When the cases of electric multipole with less strength were investigated, the results yield one or more order of magnitudes lower scavenging efficiencies.

This study also provided some indications of the variation in scavenging ability of ice crystals as they grow and aggregate. The results showed that larger ice crystals are overall more efficient scavengers than small ice particles. For larger ice crystals of bulk density 0.92 g/cm^3 (about 800 μm in diameter), the effects of electric multipoles are minimal for aerosol particles larger than a few micrometer radius. The investigations for a low ice crystal density indicated that the effects of internal charge distributions on aerosol scavenging diminish, while the effects of net charges on ice crystals increase.

Finally, the present results for ice crystal scavenging of aerosol particles may also be interpreted as an evidence in support of the formation of internal charge distribution in growing atmospheric ice crystals. Further study is suggested to estimate the approximate characterization of freezing potential, by matching the numerical results with experimental results and adjusting the recombination factor. Some later laboratory experiments are also expected to investigate the scavenging behavior of growing ice crystals containing dilute concentrations of ionizable salts, in order to verify the predicted scavenging results by the present studies.

The authors wish to acknowledge the support of the National Oceanic and Atmospheric Administration (NOAA), through its NOAA–Nevada Cooperative Program. They would also like to thank Drs. Philip L. Altick, Steven K. Chai and M. Bradford Snyder for their helpful comments.

REFERENCES

Beard, K. V. and S. N. Grover (1974), Numerical collision efficiencies for small raindrops colliding with micron size particles, *J. Atmos. Sci.*, **31**: 543–550.

Brook, M. (1959), Laboratory studies of charge separation during ice–ice contact. *Recent Adv. in Atmos. Electricity*, Pargamon Press, London, 383–389 pp.

Burrows, D. A. and P. V. Hobbs (1970), Electrical charges on snow particles. *J. Geophys. Res.*, **75**: 4499–4505.

Carlin, J. T. (1956), M. S. Thesis, New Mexico Institute of Mining and Technology, Socorro.

Cheng, R. L. (1967), Yellowstone Field Research Expedition VII, Atmospheric Sciences Research Center, Sunny Albany, 57–59.

Cobb, A. W. and G. W. Gross (1969), Internal electric effects observed during the freezing of dilute electrolytes in water. *J. Electrochem. Soc.*, **116**: 796–804.

Finnegan, W. G. and R. L. Pitter (1988), Electric multipoles in growing ice crystals: Their role in the formation of ice crystal aggregates. *Atmos. Res.*, **22**: 235–250.

Gill, E. W. B. and G. F. Alfrey (1952), Product of electric charges on water drops. *Nature*, **169**: 203.

Gill, E. W. B. (1953), Electrification by freezing, *Brit. J. Appl. Phys., Suppl.* **2**: 16–19.

Grover, S. N. and K. V. Beard (1975), A numerical determination of the efficiency with which electrically charged cloud drops and small raindrops collide with electrically charged spherical particles of various densities. *J. Atmos. Sci.*, **32**: 2156–2165.

Grover, S. N. (1980), Numerical determination of the efficiency with which aerosol particles collide with cloud and small rain drops. Ph. D Thesis, UCLA, Los Angeles, California.

Gross, B. (1954), Theory of thermodielectric effect. *Phys. Rev.*, **94**: 1545–1551.

Gross, G. W. (1965), The Workman–Reynolds effect and ionic transfer processes at the ice–solution interface, *J. Geophys. Res.*, **70**: 2291–2300.

Gross, G. W. (1967), Ion distribution and phase boundary potentials during the freezing of very dilute ionic solutions at uniform rates. *J. Coll. Interface Sci.*, **25**: 270.

Gross, G. W. (1968), Some effect of trace inorganic on the ice / water system. In: *Trace Inorganics in Water*. Adv. in Chem. Ser. 73, Amer. Chem. Soc., Washington, D. C., 27–97.

Happel, J., and H. Brenner (1965), *Low Reynolds Number Hydrodynamics*, Prentice Hall, 553 pp.

Harimaya, T. (1975), The riming properties of snow crystals. *J. Meteor. Soc. Japan*, **53:** 384–392.

Heinmets, F. (1962), Measurements of ice–liquid interphase potentials in protonated and hydroxylated electrolytes, *Trans. Faraday Soc.*, **58:** 208–215.

Hobbs, P. V. (1974), *Ice Physics*, clarendon Press, Oxford, 837 pp.

Isono, K., M. Komobayashi and T. Takahashi (1966), A percent study of solid precipitation from convective clouds over the sea. Part III, *J. Meteor. Soc. Japan*, **44:** 227–233.

Jayaweera, K. O. L. F. and R. E. Cottis (1969), Fall velocities of plate–like and columnar crystals. *Quart. J. Roy. Meteor. Soc.*, **95:** 703–709.

Jayaweera, K. O. L. F (1972), An equivalent disc for calculating the terminal velocities of plate–like ice crystals. *J. Atmos. Sci.*, **29:** 596–598.

Junge, C. E. (1963), Air Chemistry and Radioactivity, Academic Press, New York, 382 pp.

Kajikawa, M. (1972), Measurement of falling velocities of individual snow crystals. *J. Meteor. Soc. Japan*, **52:** 328–336.

Kikuchi, K. (1973), On the polarity of the electric charges on snow crystals of various shapes. *J. Meteor. Soc. Japan*, **51:** 337–345.

kikuchi, K. and H. Uyeda (1979), Cloud droplets and raindrops collected and frozen on natural snow crystals. *J. Meteor. Soc. Japan*, **57:** 273–280.

Kuroda, T. (1982), Growth kinetics of ice single crystal from vapor phase and variation of its growth form. *J. Met. Soc. Japan*, **60:** 520–534.

Kuroda, R. and R. Lacmann (1982), Growth kinetics of ice from the vapor phase and its growth forms. *J. Crystal Growth*, **56:** 189–205.

Langmuir, I. (1948), The production of rain by a chain reaction in cumulus clouds at temperatures above freezing. *J. Meteor.*, **47:** 2426–2434.

LeFebre, V. (1967), The freezing potential of electrolytic solutions. *J. Atmos. Sci.*, **25:** 263.

Levi, L. and O. Milman (1966), Freezing potential of electrolytic solutions. *J. Atmos. Sci.*, **23:** 182.

List, R. and R. S. Schemenauer (1971), Free fall behavior of planar snow crystals, conical graupel and small hail. *J. Atmos. Sci.*, **28:** 110–115.

Locatelli, J. D. and P. V. Hobbs (1974), Fall speeds and masses of solid precipitation particles. *J. Geophys. Res.*, **79:** 2185–2197.

Lodge, J. P., M. L. Baker and J. M. Pierrard (1956), Observations on ion separation in dilute solutions by freezing, *J. Chem. Phys.*, **24:** 715–719.

Magono, G. and K. Kikuchi (1961), On the electrical charge of relatively large natural cloud particles. *J. Meteor. Soc. Japan*, **39:** 258–268.

Magono, C. and S. Tazawa (1972), Aggregation phenomena of ice crystals. *J. Met. Soc. Japan*, **50:** 489–495.

Magono, C. and R. Iwabuchi (1979), The electric charge on individual ice crystals. *J. Meteor. Soc. Japan*, **57:** 207–212.

Martin, J. J., P. K. Wang and H. R. Pruppacher (1980), A theoretical determination of the efficiency with which aerosol particles are collected by simple ice plates. *J. Atmos. Sci.*, **37:** 1628–1638.

Martin, J. J., P. K. Wang, H. R. Pruppacher and R. L. Pitter (1981), A numerical study of the effect of eletric charge on the efficiency with which planar ice crystals collect supercooled cloud drops. *J. Atmos. Sci.*, **38:** 2463–2469.

Masliyah, J. H. and N. Epstein (1970), Numerical study of steady flow past spheroids. *J. Fluid Mech.*, **44:** 493–512.

Michael, P (1966), Steady motion of a disk in a viscous fluid. *Phys. Fluids*, **9:** 466–471.

Miller, N. L. and P. K. Wang (1989), Theoretical determination of the efficiency of aerosol particle collection by falling columnar ice crystals. *j. Atmos. Sci.*, **46:** 1656–1663.

Neiburger, M. (1967), Collision efficiency of nearly equal cloud drops. *Mon. Wea. Rev.*, **95:** 917–920.

Oberbeck, A. (1876), Uber die stationare Flussigkeitsbewegungen mit Berucksichtigung der inneren reibung. *J. Reine Angew. Math.* (Crelle's J. Math), **81:** 62–80.

Odencrantz, F. K. (1968), Modification of habit and charge of ice crystals by vapor contamination. *J. Atmos. sci.*, **25:** 237–238.

Parreira, H. C. and A. J. Eydt (1965), Electric potentials generated by freezing of dilute aqueous solutions. *Nature*, **208:** 33.

Pitter, R. L., H. R. Pruppacher and A. E. Hamielec (1973), A numerical study of the flow past a thin oblate spheroid at low and intermediate Reynolds numbers. *J. Atmos. Sci.* **30:** 125–134.

Pitter, R. L. and H. R. Pruppacher (1974), A numerical investigation of collision efficiencies of simple ice plates colliding with supercooled drops. *J. Atmos. Sci.*, **31:** 551–559.

Pitter, R. L. (1977), Scavenging efficiency of electrically charged thin ice plates and spheroidal aerosol particles. *J. Atmos. Sci.*, **34:** 1797–1800.

Prodi, F. (1976), Scavenging of aerosol particles by growing ice crystals. Preprints of Int. Conf. on cloud Phys., July, 1976, Boulder, Colorado, 70–75.

Pruppacher, H. R., E. H. Steinberger and R. L. Wang (1968), On the electrical effects that accompany the spontaneous growth of ice in supercooled aqueous solutions. *J. Geophys. Res.*, **73:** 571.

Pruppacher, H. R. and J. D. klett (1978), Microphysics of Clouds and Precipitation. D. Reidel Publishing Co., Holland, 714 pp.

Reynolds, S. E., M. Brook and M. F. Gourley (1957), Thunderstorm charge separation. *J. Meteor.*, **14:** 426–436.

Rimon, Y. (1969), Numerical solution of the incompressible time dependent viscous flow past a thin oblate spheroid. Rept. no. 2955, Dept. of the Navy, Naval Ship Research and development Center, washington, D. C., 44 pp.

Rimon, Y. and H. J. Lugt (1969), Laminar flow past oblate spheroids of various thicknesses. *Phys. Fluids*, **12:** 2465–2472.

Schlamp, R. J., H. R. Pruppacher and A. E. Hamielec (1975), a numerical investigation of the efficiency with which simple columnar ice crystals collide with supercooled water drops. *J. Atmos. Sci.*, **32:** 2330–2337.

Shafrir, U. and M. Neiburger (1963), Collision efficiencies of two spheres falling in a viscous medium. *J. Geophys. Res.*, **68:** 4141–4147.

Shafrir, U. and T. Gal-Chen (1971), Anumerical study of collision efficiencies and coalescence parameters for droplet pairs with radii up to 300 microns. *J. Atmos. Sci.*, **28:** 741–751.

Smith-Johanson, R. i. (1969), Ice crystal agglomeration: T-formation. *J. Atmos. Sci.*, **26:** 523–534.

Stark, P. A. (1970), *Introduction to Numerical Methods*, Macmillan Publishing Co., inc., New York, 273 pp.

Stickel, P. G. (1982), Observation of ice crystal aggregation at temperature near −50°C. Preprints of AMS Conference on Cloud Physics, Chicago, 226–229.

Takahashi, T. (1973), Measurements of electric charge on cloud drops, drizzle drops and simulated snow crystals. *Rev. Geophys. Space Phys.*, **11:** 903–924.

Wang, P. K. and H. R. Pruppacher (1980), On the efficiency with which aerosol particles of radius less than 1 μm are collected by columnar ice crystals. *Pure Appl. Geophys.*, **118:** 1090–1108.

Wang, P. K. (1985), A convective diffusion model for the scavenging of submicron aerosol particles by snow crystals of arbitrary shapes. *J. Rech. Atmos.*, **19:** 185–191.

Wilkins, R. I. and A. H. Auer (1970), Riming properties of hexagonal ice crystals. Preprints Conf. Cloud Physics, Fort Collins, *Amer. Meteor. Soc.*, 81–82.

Workman, E. J. and S. E. Reynolds (1950), Electric phenomena occurring during the freezing of dilute aqueous solutions and their possible relationship to thunderstorm electricity. *Phys. Rev.*, **78:** 254–259.